# Fresnel incoherent correlation hologram-a review

**Invited Paper**

**Joseph Rosen, Barak Katz[1], and Gary Brooker[2**]**

[1] *Department of Electrical and Computer Engineering, Ben-Gurion University of the Negev, P.O. Box 653, Beer-Sheva 84105, Israel*

[2] *Johns Hopkins University Microscopy Center, Montgomery County Campus, Advanced Technology Laboratory, Whiting School of Engineering, 9605 Medical Center Drive Suite 240, Rockville, MD 20850, USA*

[*] *E-mail: rosen@ee.bgu.ac.il;* [**] *e-mail: gbrooker@jhu.edu*

Received July 17, 2009

Holographic imaging offers a reliable and fast method to capture the complete three-dimensional (3D) information of the scene from a single perspective. We review our recently proposed single-channel optical system for generating digital Fresnel holograms of 3D real-existing objects illuminated by incoherent light. In this motionless holographic technique, light is reflected, or emitted from a 3D object, propagates through a spatial light modulator (SLM), and is recorded by a digital camera. The SLM is used as a beam-splitter of the single-channel incoherent interferometer, such that each spherical beam originated from each object point is split into two spherical beams with two different curve radii. Incoherent sum of the entire interferences between all the couples of spherical beams creates the Fresnel hologram of the observed 3D object. When this hologram is reconstructed in the computer, the 3D properties of the object are revealed.

*OCIS codes:* 100.6640, 210.4770, 180.1790.
*doi: 10.3788/COL20090712.0000.*

## 1. Introduction

Holography is an attractive imaging technique as it offers the ability to view a complete three-dimensional (3D) volume from one image. However, holography is not widely applied to the regime of white-light imaging, because white-light is incoherent and creating holograms requires a coherent interferometer system. In this review, we describe our recently invented method of acquiring incoherent digital holograms. The term incoherent digital hologram means that incoherent light beams reflected or emitted from real-existing objects interfere with each other. The resulting interferogram is recorded by a digital camera and digitally processed to yield a hologram. This hologram is reconstructed in the computer so that 3D images appear on the computer screen.

The oldest methods of recording incoherent holograms have made use of the property that every incoherent object is composed of many source points, each of which is self-spatial coherent and can create an interference pattern with light coming from the point's mirrored image. Under this general principle, there are various types of holograms[1−8], including Fourier[2,6] and Fresnel holograms[3,4,8]. The process of beam interfering demands high levels of light intensity, extreme stability of the optical setup, and a relatively narrow bandwidth light source. More recently, three groups of researchers have proposed computing holograms of 3D incoherently illuminated objects from a set of images taken from different points of view[9−12]. This method, although it shows promising prospects, is relatively slow since it is based on capturing tens of scene images from different view angles. Another method is called scanning holography[13−15], in which a pattern of Fresnel zone plates (FZPs) scans the object such that at each and every scanning position, the light intensity is integrated by a point detector. The overall process yields a Fresnel hologram obtained as a correlation between the object and FZP patterns. However, the scanning process is relatively slow and is done by mechanical movements. A similar correlation is actually also discussed in this review, however, unlike the case of scanning holography, our proposed system carries out a correlation without movement.

## 2. General properties of Fresnel holograms

This review concentrates on the technique of incoherent digital holography based on single-channel incoherent interferometers, which we have been involved in their development recently[16−19]. The type of hologram discussed here is the digital Fresnel hologram, which means that a hologram of a single point has the form of the well-known FZP. The axial location of the object point is encoded by the Fresnel number of the FZP, which is the technical term for the number of the FZP rings along the given radius.

To understand the operation principle of any general Fresnel hologram, let us look on the difference between regular imaging and holographic systems. In classical imaging, image formation of objects at different distances from the lens results in a sharp image at the image plane for objects at only one position from the lens, as shown in Fig. 1(a). The other objects at different distances from the lens are out of focus. A Fresnel holographic system, on the other hand, as depicted in Fig. 1(b), projects a set of rings known as the FZP onto the plane of the image for each and every point at every plane of the object being viewed. The depth of the points is encoded by the density of the rings such that points which are closer to the system project less dense rings than distant points. Because of this encoding method, the 3D information in the volume being imaged is recorded into the recording medium. Thus once the patterns are decoded, each plane in the image space reconstructed from a Fresnel hologram is in focus at a different axial distance. The encoding is accomplished by the presence of a holographic system in the image path. At this point it should be noted that this graphical description of projecting FZPs by every object point actually expresses the mathematical two-dimensional (2D) correlation (or convolution) between the object function and the FZP. In other words, the methods of creating Fresnel holograms are different from each other by the way they spatially correlate the FZP with the scene. Another issue to note is that the correlation should be done with a FZP that is somehow "sensitive" to the axial locations of the object points. Otherwise, these locations are not encoded into the hologram. The system described in this review satisfies the condition that the FZP is dependent on the axial distance of each and every object point.

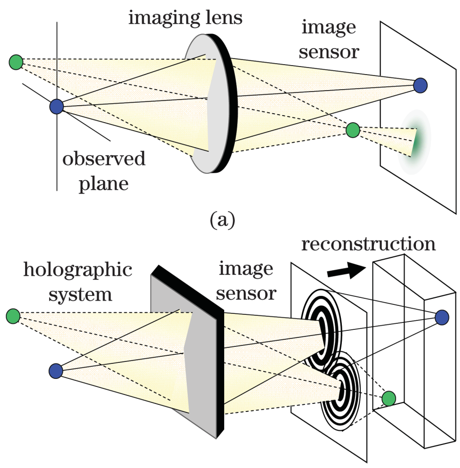


Fig. 1. Comparison between the Fresnel holography principle and conventional imaging. (a) Conventional imaging system; (b) fresnel holography system.

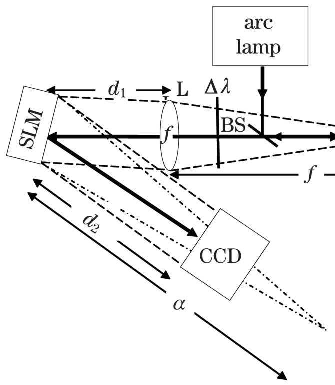


Fig. 2. Schematic of FINCH recorder[16]. BS: beam splitter; L is a spherical lens with focal length $f = 25$ cm; $\Delta\lambda$ indicates a chromatic filter with a bandwidth of $\Delta\lambda = 60$ nm.

This means that indeed points, which are closer to the system, project FZP with less cycles per radial length than distant points, and by this condition the holograms can actually image the 3D scene properly.

The FZP is a sum of at least three main functions, i.e., a constant bias, a quadratic phase function and its complex conjugate. The object function is actually correlated with all these three functions. However, the useful information, with which the holographic imaging is realized, is the correlation with just one of the two quadratic phase functions. The correlation with the other quadratic phase function induces the well-known twin image. This means that the detected signal in the holographic system contains three superposed correlation functions, whereas only one of them is the required correlation between the object and the quadratic phase function. Therefore, the digital processing of the detected image should contain the ability to eliminate the two unnecessary terms.

To summarize, the definition of Fresnel hologram is any hologram that contains at least a correlation (or convolution) between an object function and a quadratic phase function. Moreover, the quadratic phase function must be parameterized according to the axial distance of the object points from the detection plane. In other words, the number of cycles per radial distance of each quadratic phase function in the correlation is dependent on the $z$ distance of each object point. In the case that the object is illuminated by a coherent wave, this correlation is the complex amplitude of the electromagnetic field directly obtained, under the paraxial approximation[20], by a free propagation from the object to the detection plane. However, we deal here with incoherent illumination, for which an alternative method to the free propagation should be applied. In fact, in this review we describe such method to get the desired correlation with the quadratic phase function, and this method indeed operates under incoherent illumination.

The discussed incoherent digital hologram is dubbed Fresnel incoherent correlation hologram (FINCH)[16−18]. The FINCH is actually based on a single-channel on-axis incoherent interferometer. Like any Fresnel holography, in the FINCH the object is correlated with a FZP, but the correlation is carried out without any movement and without multiplexing the image of the scene. Section 3 reviews the latest developments of the FINCH in the field of color holography, microscopy, and imaging with a synthetic aperture.

## 3. Fresnel incoherent correlation holography

In this section we describe the FINCH – a method of recording digital Fresnel holograms under incoherent illumination. Various aspects of the FINCH have been described in Refs. [16-19], including FINCH of reflected white light[16], FINCH of fluorescence objects[17], a FINCH-based holographic fluorescence microscope[18], and a hologram recorder in a mode of a synthetic aperture[19]. We briefly review these works in the current section.

Generally, in the FINCH system the reflected incoherent light from a 3D object propagates through a spatial light modulator (SLM) and is recorded by a digital camera. One of the FINCH systems[16] is shown in Fig. 2. White-light source illuminates a 3D scene, and the reflected light from the objects is captured by a charge-coupled device (CCD) camera after passing through a lens L and the SLM. In general, we regard the system as an incoherent interferometer, where the grating displayed on the SLM is considered as a beam splitter. As is common in such cases, we analyze the system by following its response to an input object of a single infinitesimal point. Knowing the system's point spread function (PSF) enables one to realize the system operation for any general object. Analysis of a beam originated from a narrow-band infinitesimal point source is done by using Fresnel diffraction theory[20], since such a source is coherent by definition.

A Fresnel hologram of a point object is obtained when the two interfering beams are two spherical beams with different curvatures. Such a goal is achieved if the SLM's reflection function is a sum of, for instance, constant and quadratic phase functions. When a plane wave hits the SLM, the constant term represents the reflected plane wave, and the quadratic phase term is responsible for the reflected spherical wave.

A point source located at some distance from a spherical positive lens induces on the lens plane a diverging spherical wave. This wave is split by the SLM into two different spherical waves which propagate toward the CCD at some distance from the SLM. Consequently, in the CCD plane, the intensity of the recorded hologram is a sum of three terms: two complex-conjugated quadratic phase functions and a constant term. This result is the PSF of the holographic recording system.

For a general 3D object illuminated by a narrowband incoherent illumination, the intensity of the recorded hologram is an integral of the entire PSFs, over all object intensity points. Besides a constant term, the hologram expression contains two terms of correlation between an object and a quadratic phase, $z$-dependent, function. In order to remain with a single correlation term out of the three terms, we follow the usual procedure of on-axis digital holography[14,16−19]. Three holograms of the same object are recorded with different phase constants. The final hologram is a superposition of the three holograms containing only the desired correlation between the object function and a single $z$-dependent quadratic phase. A 3D image of the object can be reconstructed from the hologram by calculating the Fresnel

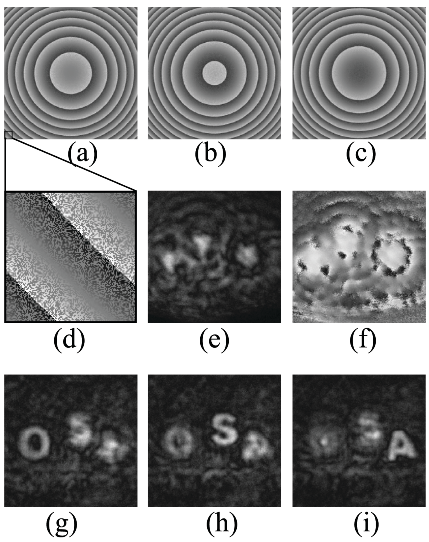


Fig. 3. (a) Phase distribution of the reflection masks displayed on the SLM, with $\theta = 0°$, (b) $\theta = 120°$, (c) $\theta = 240°$. (d) Enlarged portion of (a) indicating that half (randomly chosen) of the SLM's pixels modulate light with a constant phase. (e) Magnitude and (f) phase of the final on-axis digital hologram. (g) Reconstruction of the hologram of the three characters at the best focus distance of 'O'. (h) Same reconstruction at the best focus distance of 'S', and (i) of 'A'[16].

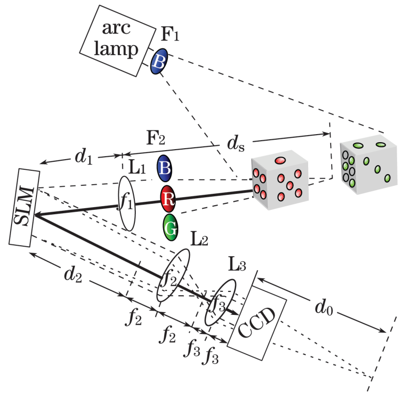


Fig. 4. Schematics of the FINCH color recorder[17]. $L_1$, $L_2$, $L_3$ are spherical lenses and $F_1$, $F_2$ are chromatic filters.

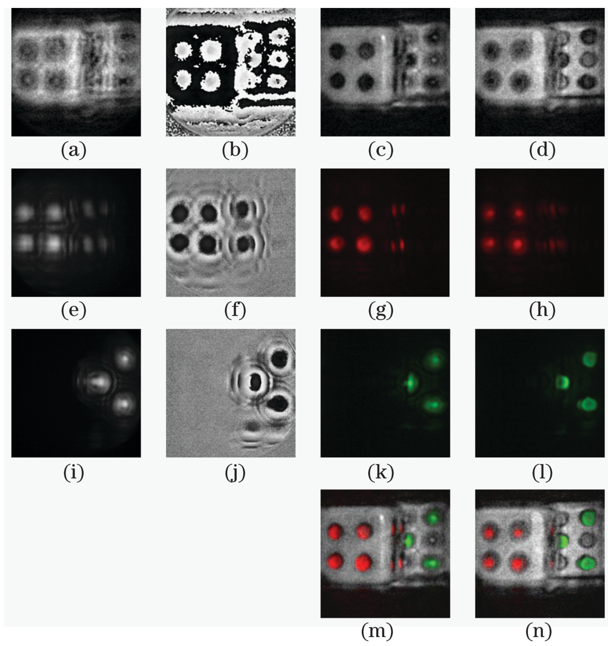


Fig. 5. (a) Magnitude and (b) phase of the complex Fresnel hologram of the dice. Digital reconstruction of the non-fluorescence hologram: (c) at the face of the red dots on the die, and (d) at the face of the green dots on the die. (e) Magnitude and (f) phase of the complex Fresnel hologram of the red dots. Digital reconstruction of the red fluorescence hologram: (g) at the face of the red dots on the die, and (h) at the face of the green dots on the die. (i) Magnitude and (j) phase of the complex Fresnel hologram of the green dots. Digital reconstruction of the green fluorescence hologram: (k) at the face of the red dots on the die, and (l) at the face of the green dots on the die. Composition of (c), (g), (k) and that of (d), (h), (l) are depicted in (m) and (n), respectively[17].

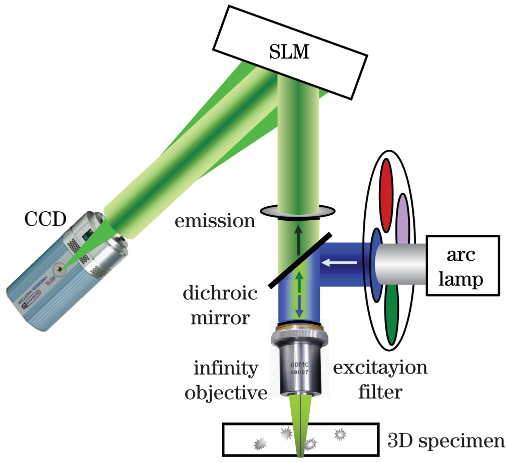


Fig. 6. FINCHSCOPE schematic in upright fluorescence microscope[18].

propagation formula.

The system shown in Fig. 2 has been used to record the three holograms[16]. The SLM has been phase-only, and as so, the desired sum of two phase functions (which is no longer a pure phase) cannot be directly displayed on this SLM. To overcome this obstacle, the quadratic phase function has been displayed randomly on only half of the SLM pixels, and the constant phase has been displayed on the other half. The randomness in distributing the two phase functions has been required because organized non-random structure produces unnecessary diffraction orders, therefore, results in lower interference efficiency. The pixels are divided equally, half to each diffractive element, to create two wavefronts with equal energy. By this method, the SLM function becomes a good approximation to the sum of two phase functions. The phase distributions of the three reflection masks displayed on the SLM, with phase constants of 0°, 120° and 240°, are shown in Figs. 3(a), (b) and (c), respectively.

Three white-on-black characters $i$th the same size of 2×2 (mm) were located at the vicinity of rear focal point of the lens. 'O' was at $z=-24$ mm, 'S' was at $z=-48$ mm, and 'A' was at $z=-72$ mm. These characters were illuminated by a mercury arc lamp. The three holograms, each for a different phase constant of the SLM, were recorded by a CCD camera and processed by a computer. The final hologram was calculated according to the superposition formula[14] and its magnitude and phase distributions are depicted in Figs. 3(e) and (f), respectively. The hologram was reconstructed in the computer by calculating the Fresnel propagation toward various $z$ propagation distances. Three different reconstruction planes are shown in Figs. 3(g), (h), and (i). In each plane, a different character is in focus as is indeed expected from a holographic reconstruction of an object with a volume.

In Ref. [17], the FINCH has been capable to record multicolor digital holograms from objects emitting fluorescent light. The fluorescent light, specific to the emission wavelength of various fluorescent dyes after excitation of 3D objects, was recorded on a digital monochrome camera after reflection from the SLM. For each wavelength of fluorescent emission, the camera sequentially records three holograms reflected from the SLM, each with a different phase factor of the SLM's function. The three holograms are again superposed in the computer to create a complex-valued Fresnel hologram of each fluorescent emission without the twin image problem. The holograms for each fluorescent color are further combined in a computer to produce a multicolored fluorescence hologram and 3D color image.

An experiment showing the recording of a color fluorescence hologram was carried out[17] on the system in Fig. 4. The phase constants of 0°, 120°, and 240° were introduced into the three quadratic phase functions. The magnitude and phase of the final complex hologram, superposed from the first three holograms, are shown in Figs. 5(a) and (b), respectively. The reconstruction from the final hologram was calculated by using the Fresnel propagation formula[20]. The results are shown at the plane of the front face of the front die (Fig. 5(c)) and the plane of the front face of the rear die (Fig. 5(d)). Note that in each plane a different die face is in focus as is indeed expected from a holographic reconstruction of an object with a volume. The second three holograms were recorded via a red filter in the emission filter slider $F_2$ which passed 614−640 nm fluorescent light wavelengths with a peak wavelength of 626 nm and a full-width at half-maximum, of 11 nm (FWHM). The magnitude and phase of the final complex hologram, superposed from the 'red' set, are shown in Figs. 5(e) and (f), respectively. The reconstruction results from this final hologram are shown in Figs. 5(g) and (h) at the same planes as those in Figs. 5(c) and (d), respectively. Finally, an additional set of three holograms was recorded with a green filter in emission filter slider $F_2$, which passed 500−532 nm fluorescent light wavelengths with a peak wavelength of 516 nm and a FWHM of 16 nm. The magnitude and phase of the final complex hologram, superposed from the 'green' set, are shown in Figs. 5(i) and (j), respectively. The reconstruction results from this final hologram are shown in Figs. 5(k) and (l) at the same planes as those in Fig. 5(c) and (d), respectively. Compositions of Figs. 5(c), (g), and (k) and Figs. 5(d), (h), and (l) are depicted in Figs. 5(m) and (n), respectively. Note that all the colors in Fig. 5 (colorful online) are pseudo-colors. These last results yield a complete color 3D holographic image of the object including the red and green fluorescence. While the optical arrangement in this demonstration has not been optimized for maximum resolution, it is important to recognize that even with this simple optical arrangement, the resolution is good enough to image the fluorescent emissions with good fidelity and to obtain good reflected light images of the dice. Furthermore, in the reflected light images in Figs. 5(c) and (m), the system has been able to detect a specular reflection of the illumination from the edge of the front dice.

Another system to be reviewed here is the first demonstration of a motionless microscopy system (FINCHSCOPE) based upon the FINCH and its use in recording high-resolution 3D fluorescent images of biological specimens[18]. By using high numerical aperture (NA) lenses, a SLM, a CCD camera, and some simple filters, FINCHSCOPE enables the acquisition of 3D microscopic images without the need for scanning.

A schematic diagram of the FINCHSCOPE for an upright microscope equipped with an arc lamp source

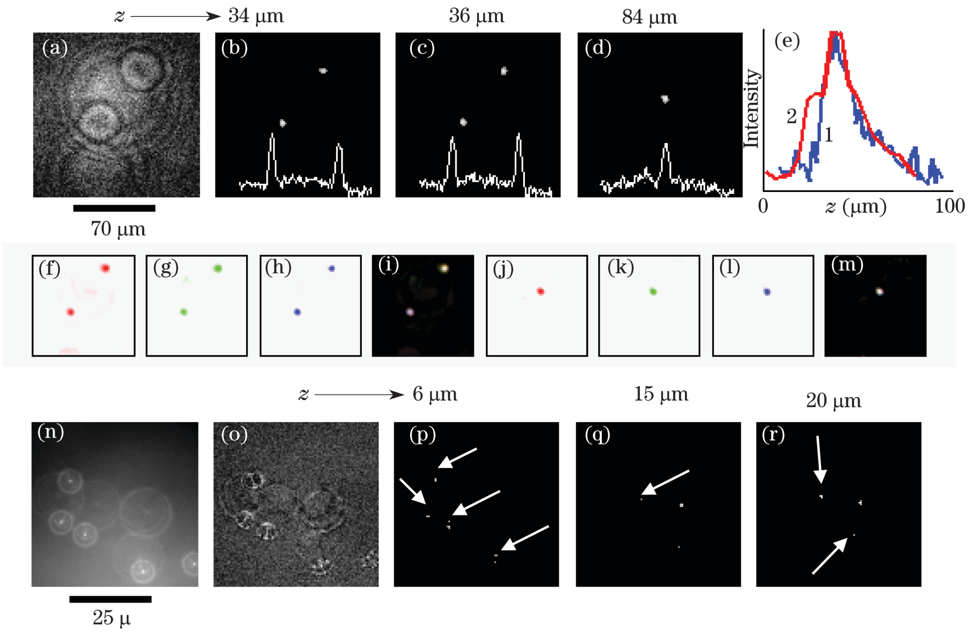


Fig. 7. FINCHSCOPE holography of polychromatic beads. (a) Magnitude of the complex hologram 6-$\mu$m beads. Images reconstructed from the hologram at $z$ distances of (b) 34 $\mu$m, (c) 36 $\mu$m, and (d) 84 $\mu$m. Line intensity profiles between the beads are shown at the bottom of panels (b)–(d). (e) Line intensity profiles along the $z$ axis for the lower bead from reconstructed sections of a single hologram (line 1) and from a widefield stack of the same bead (28 sections, line 2). Beads (6 $\mu$m) excited at 640, 555, and 488 nm with holograms reconstructed (f)–(h) at plane (b) and (j)–(l) at plane (d). (i) and (m) are the combined RGB images for planes (b) and (d), respectively. (n)–(r) Beads (0.5 $\mu$m) imaged with a 1.4-NA oil immersion objective: (n) holographic camera image; (o) magnitude of the complex hologram; (p)–(r) reconstructed image at planes 6, 15, and 20 $\mu$m. Scale bars indicate image size[18].

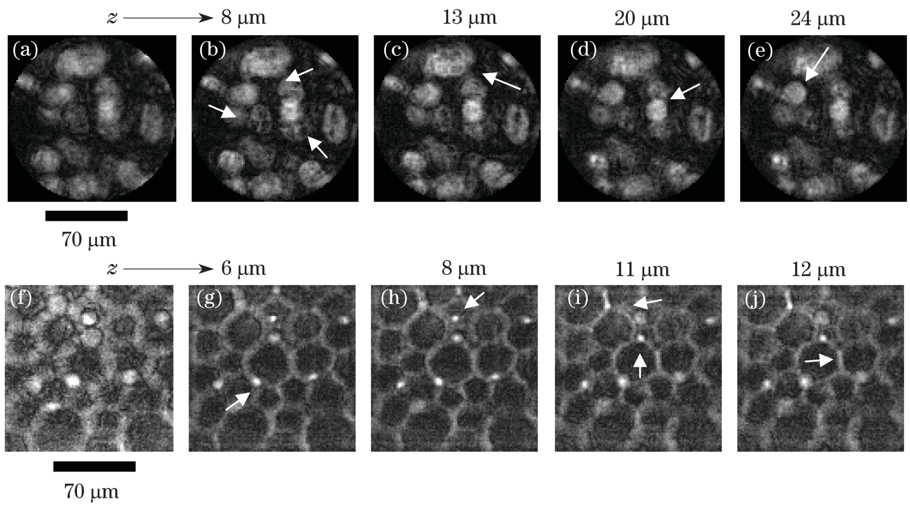


Fig. 8. FINCHSCOPE fluorescence sections of pollen grains and *Convallaria rhizom*. The arrows point to the structures in the images that are in focus at various image planes. (b)–(e) Sections reconstructed from a hologram of mixed pollen grains. (g)–(j) Sections reconstructed from a hologram of *Convallaria rhizom*. (a),(f) Magnitudes of the complex holograms from which the respective image planes are reconstructed. Scale bars indicate image size[18].

is shown in Fig. 6. The beam of light that emerges from an infinity-corrected microscope objective transforms each point of the object being viewed into a plane wave, thus satisfying the first requirement of FINCH[16]. A SLM and a digital camera replace the tube lens, reflective mirror, and other transfer optics normally present in microscopes. Because no tube lens is required, infinity-corrected objectives from any manufacturer can be used. A filter wheel was used to select excitation wavelengths from a mercury arc lamp, and the dichroic mirror holder and the emission filter in the microscope were used to direct light to and from the specimen through an infinity-corrected objective.

The ability of the FINCHSCOPE to resolve multicolor fluorescent samples was evaluated by first imaging polychromatic fluorescent beads. A fluorescence bead slide with the beads separated on two separate planes was constructed. FocalCheck polychromatic beads (6 $\mu$m) were used to coat one side of a glass microscope slide and a glass coverslip. These two surfaces were juxtaposed and held together at a distance from one another of ~50 $\mu$m with optical cement. The beads were sequentially excited at 488-, 555-, and 640-nm center wavelengths (10 – 30 nm bandwidths) with emissions recorded at 515 – 535, 585 – 615, and 660 – 720 nm, respectively. Figures 7(a)–(d) show reconstructed image planes from 6 $\mu$m beads excited at 640 nm and imaged on the FINCHSCOPE with a Zeiss PlanApo 20×, 0.75 NA objective. Figure 7(a) shows the magnitude of the complex hologram, which contains all the information about the location and intensity of each bead at every plane in the field. The Fresnel reconstruction from this hologram was selected to yield 49 planes of the image, 2-$\mu$m apart. Two beads are shown in Fig. 7(b) with only the lower bead exactly in focus. Figure 7(c) is 2 $\mu$m into the field in the$z$-direction, and the upper bead is now in focus, with the lower bead slightly out of focus. The focal difference is confirmed by the line profile drawn between the beads, showing an inversion of intensity for these two beads between the planes. There is another bead between these two beads, but it does not appear in Figs. 7(b) or (c) (or in the intensity profile), because it is 48 $\mu$m from the upper bead; it instead appears in Fig. 7(d) (and in the line profile), which is 24 sections away from the section in Fig. 7(c). Notice that the beads in Figs. 7(b) and (c) are no longer visible in Fig. 7(d). In the complex hologram in Fig. 7(a), the small circles encode the close beads and the larger circles encode the distant central bead. Figure 7(e) shows that the $z$-resolution of the lower bead in Fig. 7(b), reconstructed from sections created from a single hologram (curve 1), is at least comparable to data from a widefield stack of 28 sections (obtained by moving the microscope objective in the $z$-direction) of the same field (curve 2). The co-localization of the fluorescence emission was confirmed at all excitation wavelengths and at extreme $z$ limits, as shown in Figs. 7(f) – (m) for the 6-$\mu$m beads at the planes shown in Figs. 7(b) ((f) – (i)) and (d) ((j) – (m)). In Figs. 7(n) – (r), 0.5-$\mu$m beads imaged with a Zeiss PlanApo ×63 1.4 NA oil-immersion objective are shown. Figure 7(n) presents one of the holograms captured by the camera and Fig. 7(o) shows the magnitude of the complex hologram. Figures 7(p) – (r) show different planes (6, 15, and 20 $\mu$m, respectively) in the bead specimen after reconstruction from the complex hologram of image slices in 0.5-$\mu$m steps. Arrows show the different beads visualized in different $z$ image planes. The computer reconstruction along the $z$-axis of a group of fluorescently labeled pollen grains is shown in Figs. 8(b) – (e). As is expected from a holographic reconstruction of a 3D object with volume, any number of planes can be reconstructed. In this example, a different pollen grain was in focus in each transverse plane reconstructed from the complex hologram whose magnitude is shown in Fig. 8(a). In Figs. 8(b) – (e), the values of $z$ are 8, 13, 20, and 24 $\mu$m, respectively. A similar experiment was performed with the autofluorescent *Convallaria rhizom* and the results are shown in Figs. 8(g) – (j) at planes 6, 8, 11, and 12 $\mu$m.

The most recent development in FINCH is a new lensless incoherent holographic system operating in a synthetic aperture mode[19]. Synthetic aperture is a well-known super-resolution technique which extends the resolution capabilities of an imaging system beyond the theoretical Rayleigh limit dictated by the system's actual aperture. Using this technique, several patterns acquired by an aperture-limited system, from various locations, are tiled together to one large pattern which could be captured only by a virtual system equipped with a much wider synthetic aperture.

The use of optical holography for synthetic aperture is usually restricted to coherent imaging[21−23]. Therefore, the use of this technique is limited only to those applications in which the observed targets can be illuminated by a laser. Synthetic aperture carried out by a combination of several off-axis incoherent holograms in scanning holographic microscopy has been demonstrated by Indebetouw *et al*[24]. However, this method is limited to microscopy only, and although it is a technique of recording incoherent holograms, a specimen should also be illuminated by an interference pattern between two laser beams.

Our new scheme of holographic imaging of incoherently illuminated objects is dubbing a synthetic aperture with Fresnel elements (SAFE). This holographic lensless system contains only a SLM and a digital camera. SAFE has an extended synthetic aperture in order to improve the transverse and axial resolutions beyond the classic limitations. The term synthetic aperture, in the present context, means time (or space) multiplexing of several Fresnel holographic elements captured from various viewpoints by a system with a limited real aperture. The synthetic aperture is implemented by shifting the SLM-camera set, located across the field of view, between several viewpoints. At each viewpoint, a different mask is displayed on the SLM, and a single element of the Fresnel hologram is recorded (Fig. 9). The various elements, each of which is recorded by the real aperture system during the capturing time, are tiled together so that the final mosaic hologram is effectively considered as being captured from a single synthetic aperture, which is much wider than the actual aperture.

An example of such a system with the synthetic aperture three times wider than the actual aperture can be seen in Fig. 9. For simplicity of the demonstration, the synthetic aperture was implemented only along the horizontal axis. In principle, this concept can be generalized for both axes and for any ratio of synthetic to actual apertures. Imaging with the synthetic aperture is necessary for the cases where the angular spectrum of the light emitted from the observed object is wider than the NA of a given imaging system. In the SAFE shown in Fig. 9, the SLM and the digital camera move in front of the object. The complete Fresnel hologram of the object, located at some distance from the SLM, is a mosaic of three holographic elements, each of which is recorded from a different position by the system with the real aperture of the size $A_x \times A_y$. The complete hologram tiled from the three holographic Fresnel elements has the synthetic aperture of the size $3(\cdot A_x \times A_y)$ which is three times larger than the real aperture at the horizontal axis.

The method to eliminate the twin image and the bias term is the same as that has been used before[14,16−18];

three elemental holograms of the same object and for each point of view are recorded, each of the holograms has a different phase constant of the SLM's phase mask. The final holographic element is a specific superposition of the three recorded elements. The digital reconstruction of the final complex-valued mosaic hologram is conventionally computed by Fresnel back propagation.

SAFE has been tested in the lab by the system shown in Fig. 9. The object in this experiment is a binary grating with a cycle length of 11 lines/cm. The distance from the binary grating to the SLM is 17 cm, and that between the SLM and the CCD is 8 cm. The results of the experiments are summarized in Fig. 10. In the first experiment, we have recorded a hologram only by the actual aperture without shifting the system, in the setup shown in Fig. 9 at the time $t_2$. Figure 10(a) shows one of the three masks displayed on the SLM in this experiment. Each of the three masks has had one of the three different phase factors: 0°, 120°, or 240°. The three recorded holograms are superposed according to the same superposition equation given in Ref. [14]. Figures 10(b) and (c) are the magnitude and the phase of the superposed hologram, respectively. The resolution along the horizontal direction of the reconstructed image shown in Fig. 10(d) is damaged in the sense that the image is lacking the original horizontal gratings because the aperture is too narrow to capture the entire grating's spectral content.

In the second experiment, nine different phase masks were displayed on the SLM, three for each location of the SLM-camera set: left, central, and right. Each of the masks has had an actual aperture of 640×1080 pixels. Each of the three masks at every location has had one of the three different phase factors: 0°, 120°, or 240°. For each location of the system, the three recorded holograms have been superposed as mentioned before. Figure 10(e) represents three masks, out of nine, each of which has been displayed at different time (indicated on each mask by $t_n$, $n=1,2,3$) and at a different location of the setup along the horizontal axis. The superposed complex-valued holographic element from each system's viewpoint is stored in the computer. Upon completing the system movement along the entire synthetic aperture, all three holographic elements are tiled to a single mosaic hologram. Figures 10(f) and (g) represent the magnitude and the phase of the complete mosaic hologram, respectively. The reconstruction result of the mosaic hologram is depicted in Fig. 10(h). The grating of the observed object is seen well in the reconstructed image, indicating that the synthetic aperture is wide enough to acquire most of the spectral information of the object.

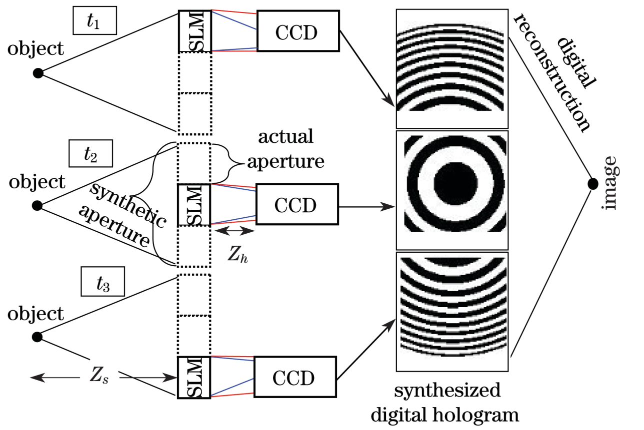


Fig. 9. Schematic of SAFE operating as a synthetic aperture radar to achieve super-resolution.

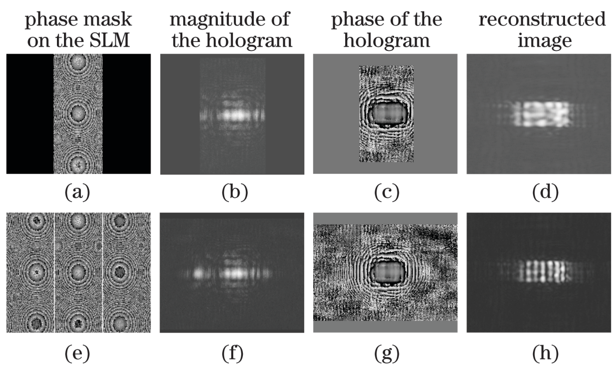


Fig. 10. Results of SAFE (a)–(d) with the actual narrow aperture, and (e)–(h) with the synthetic aperture.

## 4. Conclusion

We have reviewed a new method of generating incoherent digital Fresnel holograms. As we have shown, the holograms of FINCH are recorded by an on-axis, single-channel, incoherent interferometer. This method inherently does not scan the object neither in space nor in time. Therefore, the FINCH can generate the holograms rapidly without sacrificing the system resolution. This system offers the feature of observing a complete volume from a hologram, potentially enabling objects moving quickly in three dimensions to be tracked. The FINCH technique shows great promise in rapidly recording 3D information in any scene, independent of the illumination. In addition, we have described a rapid, non-scanning holographic fluorescence microscope that produces in-focus images at each plane in the specimen from holograms captured on a digital camera. This motionless 3D microscopy technique does not require complicated alignment or a laser. The fluorescence emission can be of relatively wide bandwidth because the optical path difference between the beams is minimal in this single-path device. Although at present each reconstructed section is not completely confocal, 3D reconstructions free of blur could be created by deconvolution of the holographic sections as is typically carried out in widefield microscopy. Time resolution is currently reduced because three holograms need to be captured sequentially. However, in the future, it will be possible to simultaneously capture all three holograms or to overcome the holographic twin image problem and capture only one hologram, as any of the three holograms contains all the essential 3D information. In the present studies, the image sections are obtained by a process of first capturing three holograms, computing the image $z$ sections from the complex hologram and then, in some cases, further enhancing them by deconvolution. This process could be simplified in the future for real-time display of the holographic image, either with a holographic display system or by algorithms that create the enhanced sections and the 3D representation directly from the single hologram. There is no need for sectioning, scanning or any mechanical movement. Therefore, this system would be expected ultimately to be faster, simpler, and more versatile than existing 3D microscopy techniques, which rely on pinhole imaging or deconvolution of stacks of widefield images. We have also demonstrated fluorescence holography using the high-NA objectives widely used in biological imaging. FINCHSCOPE is able to spatially resolve small beads, biological specimens, and different fluorescence emission colours in $x$, $y$ and $z$ planes with perfect registration. The system provides a simple, flexible, cost-effective, and powerful microscopic platform for 3D imaging.

Finally, we have demonstrated a process of recording incoherent holograms in the synthetic aperture mode. The synthetic aperture of SAFE considerably increases both the transverse and the axial resolving power. The concept of the present system can be applied to all regimes of imaging from microscopy to telescopes, and either for 2D or 3D imaging. Our demonstrations of this advance in imaging, based on a new but simple holographic principle, should open up opportunities in many life science and engineering fields, so that interesting scenes may be readily observed in three dimensions and possibly at higher resolution than with currently existing techniques.

## References


1. A. W. Lohmann, J. Opt. Soc. Am. **55,** 1555 (1965).
2. G. W. Stroke and R. C. Restrick, Appl. Phy. Lett. **7,** 229 (1965).
3. G. Cochran, J. Opt. Soc. Am. **56,** 1513 (1966).
4. P. J. Peters, Appl. Phy. Lett. **8,** 209 (1966).
5. H. R. Worthington, Jr., J. Opt. Soc. Am. **56,** 1397 (1966).
6. J. B. Breckinridge, Appl. Opt. **13,** 2760 (1974).
7. A. S. Marathay, J. Opt. Soc. Am. A **4,** 1861 (1987).
8. G. Sirat and D. Psaltis, Opt. Lett. **10,** 4 (1985).
9. Y. Li, D. Abookasis, and J. Rosen, Appl. Opt. **40,** 2864 (2001).
10. Y. Sando, M. Itoh, and T. Yatagai, Opt. Lett. **28,** 2518 (2003).
11. N. T. Shaked and J. Rosen, J. Opt. Am. A **25,** 2129 (2008).
12. J.-H. Park, M.-S. Kim, G. Baasantseren, and N. Kim, Opt. Express **17,** 6320 (2009).
13. B. W. Schilling, T.-C. Poon, G. Indebetouw, B. Storrie, K. Shinoda, Y. Suzuki, and M. H. Wu, Opt. Lett. **22,** 1506 (1997).
14. J. Rosen, G. Indebetouw, and G. Brooker, Opt. Express **14,** 4280 (2006).
15. G. Indebetouw, Chin. Opt. Lett. **7,** (2009).
16. J. Rosen and G. Brooker, Opt. Lett. **32,** 912 (2007).
17. J. Rosen and G. Brooker, Opt. Express. **15,** 2244 (2007).
18. J. Rosen and G. Brooker, Nature Photon. **2,** 190 (2008).
19. B. Katz and J. Rosen, "Incoherent holographic imaging using synthetic aperture with Fresnel elements" OSA Digital Holography Topical Meeting, Vancouver, Canada, (April 26–30, 2009).
20. J. W. Goodman, *Introduction to Fourier Optics*(2nd edn.) (McGraw-Hill, New York, 1996).
21. S. M. Beck, J. R. Buck, W. F. Buell, R. P. Dickinson, D. A. Kozlowski, N. J. Marechal, and T. J. Wright, Appl. Opt. **44,** 7621 (2005).
22. V. Mico, Z. Zalevsky, P. García-Martínez, and J. García, J. Opt. Soc. Am. A **23,** 3162 (2006).
23. L. Martínez-León and B. Javidi, Opt. Express **16,** 161 (2008).
24. G. Indebetouw, Y. Tada, J. Rosen, and G. Brooker, Appl. Opt. **46,** 993 (2007).